

Scanning Tunneling Microscopic Study with Atomic Resolution of the Dissolution of Cu(100) Electrodes in Aqueous Chloride Media

D. Wayne Suggs and Allen J. Bard*

Department of Chemistry and Biochemistry, The University of Texas at Austin, Austin, Texas 78712

Received: December 20, 1994[⊗]

In situ scanning tunneling microscopy (STM) of the dissolution of a Cu(100) electrode in aqueous chloride media (HCl) was employed to find the mechanism of reaction at the atomic level. Imaging the surface at potentials where no dissolution occurred resulted in a clear $(\sqrt{2} \times \sqrt{2})R45^\circ$ Cl structure with an observed Cl–Cl distance of 0.35 ± 0.02 nm, in agreement with previous ultrahigh vacuum surface analytical low-energy electron diffraction and Auger electron analysis studies of Cu(100) surfaces dosed with chlorine or aqueous Cl^- . Images acquired at potentials where dissolution was modest showed the preferred reaction sites were step edges with edges always retreating along the Cu(100) {100} direction. At still higher potentials, the rate increased and the reaction sites were still mainly the step edges. This work compares well with a previous STM study of Cu(111) electrodes under similar conditions, where the dissolution of the Cu(111) caused reaction along {211} step edges, which are very similar to the Cu(100) {100} step edges.

Introduction

The mechanisms of metal electrochemical surface processes, such as dissolution, corrosion, and electrodeposition, are of interest because they are theoretically and practically important.¹ Scanning tunneling microscopy (STM) has been applied successfully to the study of noble surface processes both in situ² and ex situ.³ Work in our laboratory has recently focused on in situ STM studies of the dissolution of more active metals, specifically Cu. Cu is technologically important, e.g., for printed circuit boards, and is the most stable of the active metals due to its overpotential for hydrogen evolution and lack of surface oxides in acidic solutions.⁴ Earlier we discussed the mechanism of dissolution of Cu(111) electrodes with atomic resolution in aqueous chloride solutions using in situ STM.⁵ Here, we extend this approach to an examination of Cu(100) surfaces at high resolution to compare the reaction mechanism to that found with Cu(111) under similar conditions. Our previous work on Cu(111) concluded that Cu dissolution in 10 mM HCl occurs preferentially at step edges in the {211} direction. The differing work functions for the highly kinked {211} edges vs those along the {110} direction with a smaller kink density showed that not only does each low-index plane have differing activity but that specific sites or edges on the surface can exhibit different reactivity. In this paper, Cu(100) surfaces are examined under controlled dissolution conditions. We also discuss how the mechanism at the atomic scale relates to models developed from hydrodynamic voltammetric studies of this system.

For an in situ study of this type, one must always be aware of possible tip–substrate interactions and their effect on the interpretation of images acquired during the dissolution process.³ The experiments were designed and performed to minimize such interactions. Thus, (i) the bias of the tip vs a reference electrode (V_{tip}) was maintained sufficiently positive that Cu dissolving from the substrate did not deposit on the tip. The bias between the tip and the substrate was kept small with the tip always at least 10–20 mV positive of the substrate potential. (ii) The tunneling current also controls tip–substrate separation, and the set point currents were kept small (usually 2–3 nA), although currents as high as 7–10 nA did not seem to affect the

dissolution rate or mechanism. (iii) We also checked for tip–substrate interactions by scanning a small area (usually 10–20 nm on a side) for several minutes and then by doubling the scan area. Tip-induced etching should manifest itself as an etched square area in the center of the image the size of the smaller scan. A tip-induced interaction such as this has been observed during the electrodeposition of Pb on highly oriented pyrolytic graphite (HOPG). In that study, if the tip potentials were too positive, the tip effectively prevented Pb deposition in the scanned area, and this was easily observed by increasing the scan size to reveal that the surrounding areas had Pb on the surface. Many experiments of this type were carried out in our study, and this phenomenon was not observed.

Experimental Section

Chemicals. High-purity water (Milli-Q purification system, > 18 M Ω cm) was used throughout. Potassium chloride (J. T. Baker) and hydrochloric acid (ULTREX II, J. T. Baker) were used as received.

Instrumentation. In situ images were obtained under ambient conditions with a NanoScope III STM (Digital Instruments, Santa Barbara, CA) with an electrochemical base and electrochemically etched W tips. Tips were 0.010 in. W rods (FHC, Inc., New Brunswick, ME) etched in 1 M KOH at 15 V ac. The etched tip was then rinsed with Millipore water followed by acetone. To reduce faradaic currents at the tip, the tips were insulated with polyethylene (Hot Melt Glue Stix, Arrow). The tip was coated with the polyethylene in a manner similar to that used to insulate tips with Apiezon wax.⁶ The polyethylene produced an even coating and did not contaminate the solution in the cell as quickly as clear nail polish. Contamination can be determined by degradation of the current–potential curve or by the appearance of foreign matter on STM images of clean terraces over time. The electrochemical cell was fabricated in-house from Kel-F. A 0.9 cm \times 0.9 cm Cu(100) electrode made up the base of the cell and was fitted into a milled groove in the Kel-F cell to allow the crystal to be consistently oriented in the cell. A thin slice of Teflon with a 6-mm-diameter hole served as a gasket to seal the space between the Kel-F and the electrode surface. The solution area over the electrode was connected to a small solution reservoir by a

[⊗] Abstract published in *Advance ACS Abstracts*, April 15, 1995.

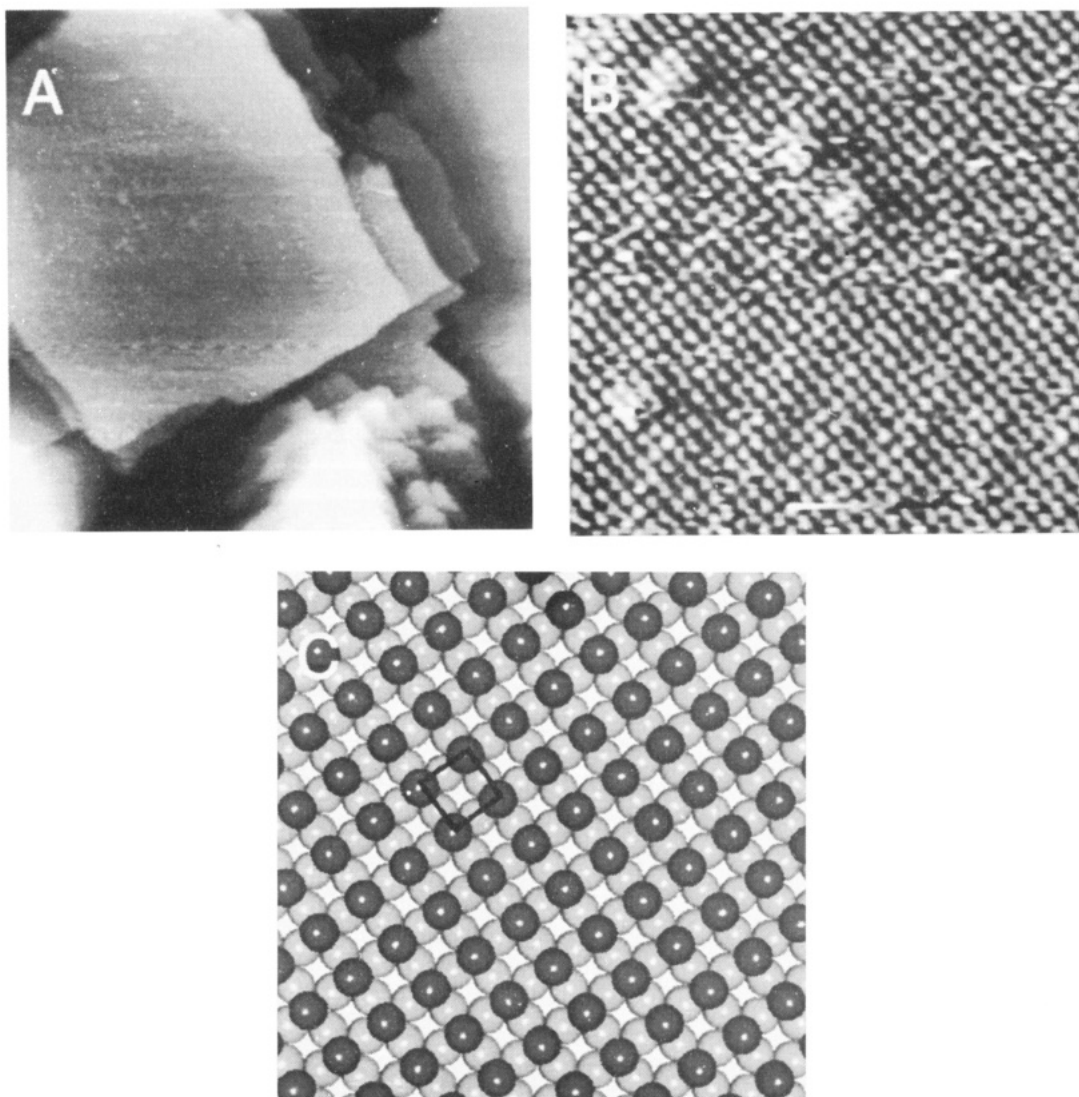


Figure 1. STM micrographs. (A) 100 nm \times 100 nm image obtained at -300 mV. $V_{\text{tip}} = 0$ mV and $i_T = 2.0$ nA. The terrace edges seen in this image, and in all of the micrographs in this paper, had step heights of 0.17 ± 0.02 nm. The total vertical distance from the darkest to the lightest area in this image is 10 nm. (B) 10 nm \times 10 nm image taken in current mode at -620 mV revealing the Cu(100) $(\sqrt{2} \times \sqrt{2})R45^\circ$ Cl adlattice structure found on all terraces. (C) 3D representation of the Cu(100) $(\sqrt{2} \times \sqrt{2})R45^\circ$ Cl structure seen in B. Cl atoms are dark and Cu atoms are light. The $(\sqrt{2} \times \sqrt{2})R45^\circ$ unit cell is outlined in black, and the directions of the step edge directions are also shown. The Cl adatoms are not drawn to scale so that the relationship of the Cl adlattice structure to the underlying copper rows can be seen. The structure has been aligned with the STM image in B, and all other STM pictures are oriented in a similar manner.

3-mm-deep trough milled in the Kel-F. A Ag/AgCl/3 M KCl reference electrode along with a 2 cm² Pt counter electrode resided in the reservoir. Potentials of the substrate Cu(100) crystal and the tip (V_{tip}) are given with respect to this reference electrode so that the Cu(100) vs tip bias is the difference between these quantities. All images were taken in the height mode, i.e., at constant current, unless otherwise noted, with different trials made on consecutive days under similar conditions. All of the images presented represent raw data and are unfiltered.

Substrate. Cu(100) single crystals disks (1 in. diameter) (a gift from Dr. Thomas Moffat, NIST) were cut into square pieces (0.9 cm \times 0.9 cm) after the substrate orientation was determined by Laue X-ray back reflection. The crystal was placed in the milled groove of the electrochemical cell with a known orientation of the substrate lattice with respect to the STM x and y scan directions. Surface preparation involved mechanical polishing down to 0.25- μm diamond paste followed by electropolishing at ~ 2 A cm⁻² for 1 s in a phosphoric acid/sulfuric acid solution (130 mL of 85% H₃PO₄, 20 mL of concentrated H₂SO₄, 60 mL of water) following published procedures.⁷ This process produced a consistent mirrorlike finish. The crystal was then

rinsed with Millipore water. A drop of water was left on the surface to protect it during transfer through air. Because of the cell configuration and experimental considerations, the solutions used in this study were not deaerated nor was oxygen excluded from the cell surroundings. This was not a problem, since the Cu etching rate could be controlled by adjustment of the electrode potential, as discussed below.

Results and Discussion

STM Imaging of Adsorbed Chloride. Imaging a freshly electropolished Cu(100) surface at open circuit in 10 mM HCl proved to be difficult due to the presence of surface oxides formed from the electropolishing step and the transfer through air. However, cycling the electrode into the dissolution region (~ 0 mV) then to the hydrogen evolution region (~ -900 mV) in 10 mM HCl resulted in a well-defined surface which was easily imaged. Figure 1A shows a typical STM micrograph of Cu(100) at -290 mV after this treatment. The orientation of the crystal is constant in all images presented, and a compass indicating the $\{100\}$ and $\{110\}$ directions is shown in Figure

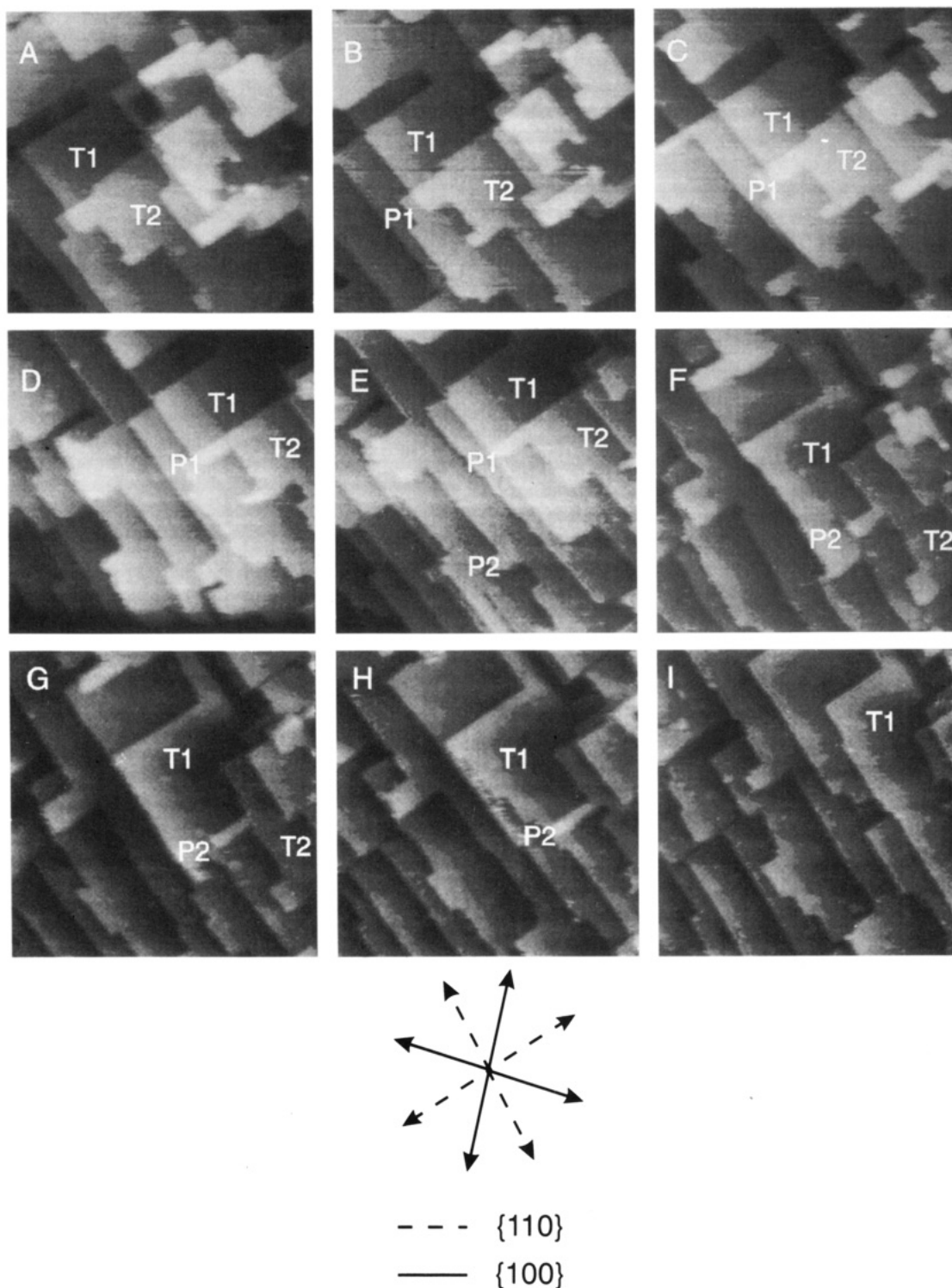


Figure 2. 45 nm \times 45 nm STM micrographs taken over a period of time showing the anodic dissolution of Cu(100) in 10 mM HCl. The time between each scan was 13 s, and key terraces are marked in each image for easy interpretation. (Note that the images are displaced slightly because of thermal drift). A compass is also drawn to show the orientation of the crystal. The potential of the Cu(100) electrode was scanned at 2 mV s⁻¹ until the dissolution was slow enough to be observed. The substrate potential for all images was -80 mV with $V_{tip} = 0$ mV and $i_T = 2$ nA.

2. Interestingly, potential cycling did not seem to affect the overall surface quality, as discussed below. Figure 1B is an atomic resolution image taken at -620 mV in the constant height mode. This structure was observed on all terraces examined. The square symmetry, the 45° rotation of the lattice relative to the known Cu(100) rows, and the interatomic spacing of 0.35 ± 0.02 nm unequivocally lead to a unit cell assignment of $(\sqrt{2} \times \sqrt{2})R45^\circ$. This structure has been previously observed on Cu(100) surfaces with low-energy electron diffraction (LEED) after vacuum dosing with Cl₂ in ultrahigh

vacuum (UHV)⁸ and following emersion from a 1 mM HCl solution.⁸ This structure has also been observed using in situ atomic force microscopy (AFM).⁹ Figure 1C is a ball model representation of the Cl adlattice and shows its orientation relative to the underlying Cu(100) surface (the Cl atoms are NOT drawn to scale so that the underlying Cu atoms can be seen). Previous LEED intensity analysis of this structure suggests that the Cl atoms sit in the 4-fold sites.¹⁰

Anodic Dissolution of Cu(100). As the potential of the Cu(100) surface is swept slowly (2 mV s⁻¹) positive in 10 mM

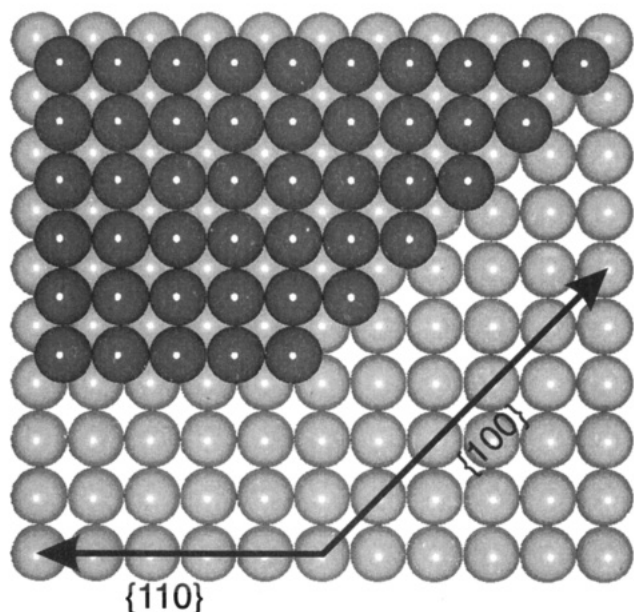


Figure 3. 3D top view of a step edge on Cu(100) illustrating the difference in geometry between steps in the $\{100\}$ and $\{110\}$ directions. The darker atoms are the top layer and the lighter are the bottom. The high density of kink sites in the $\{100\}$ directions is apparent.

HCl, pH 2.1, potentials are reached where dissolution of the Cu is slow and easily observed on the time scale of the STM imaging process. A typical dissolution experiment is shown in Figure 2. Here, the potential was scanned from -300 to -77 mV and halted. The images in this figure show some thermal drift; thus, key terraces and features are marked on the images, so one can follow the dissolution process with time. An examination of the images in Figure 2 reveals that dissolution of the Cu(100) occurs along edges in the $\{100\}$ direction. This is illustrated by the rectangular indentation in T1. The width of this indentation grows as dissolution proceeds along the $\{100\}$

sides. The $\{100\}$ edges run along the $R45^\circ$ direction, i.e., along the Cl adlattice rows, where the underlying Cu atoms are in a highly kinked arrangement. Observation of $\{110\}$ edges, i.e., along Cu rows, was rare, and when they were found, they quickly disappeared, flowing into $\{100\}$ edges. The reactivity of the $\{100\}$ edges is probably due to the density of kinks where Cu atoms are more open to attack. Figure 3 illustrates the arrangements of Cu(100) $\{100\}$ and $\{110\}$ step edges. The coordination for Cu atoms along the $\{110\}$ edge is 7 while along $\{100\}$ rows the coordination is 6. (We should note here that there are two different atomic sites along the $\{100\}$ direction, but we are only considering the outermost Cu atoms.) Note that there are steric differences between the edges. The outermost atoms along the $\{100\}$ edge are 0.36 nm apart, and the Cu–Cu separation on the $\{110\}$ edges is 0.256 nm. We can understand the absence of the $\{110\}$ edge in the images by considering the structure of the edge where two perpendicular $\{110\}$ edges meet. This is illustrated in Figure 3 at the left-hand corners of the first layer. The Cu atom at each corner would have the same coordination as the outermost Cu atom on a $\{100\}$ edge, and given that it has little steric hindrance to dissolution, it would be a likely candidate for dissolution. With the corner atom missing, we have started a new $\{100\}$ edge.

Another interesting feature seen in Figure 2 is the presence of pinned areas on the terraces. Most terraces dissolve and are not hindered. But sometimes sections of a terrace do not retreat evenly with the surrounding terrace edge. This creates a rectangular terrace which can be up to 10–20 nm in length. The length can vary, but usually the sides start to dissolve toward the back, and the pinned area separates from the parent terrace. This leaves an island which dissolves quickly. Two such pinned areas are marked in Figure 2 as P1 and P2. Note the stability over time of these pinned areas, i.e., P1 starts in part A and is gone in part F. Sometimes the corner of an edge gets pinned, and this has also been observed. Such pinning could result from impurities in the lattice or solution or from surface defects.

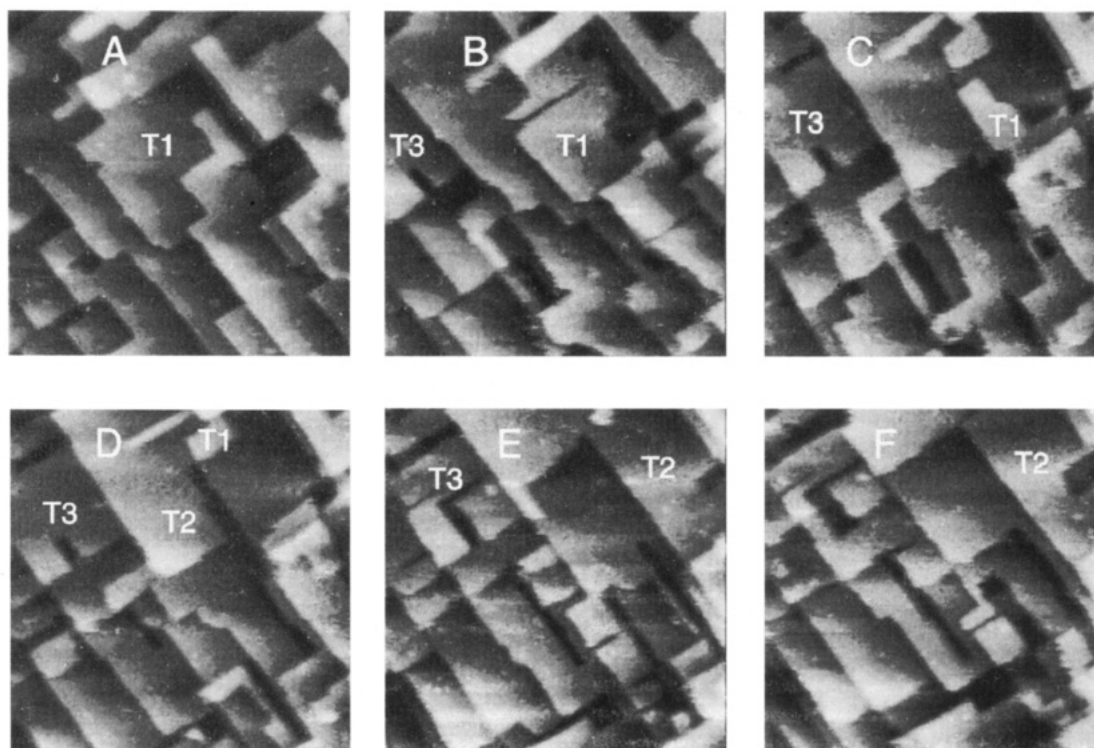


Figure 4. 45 nm \times 45 nm STM micrographs taken over a period of time showing the anodic dissolution of Cu(100) in 10 mM HCl at a higher potential than that of Figure 2. The tunneling current was 2.0 nA for all images and V_{ip} was 0 mV. Micrographs were taken at -80 mV as in Figure 2. Micrographs were taken (A) 0, (B) 25, (C) 32, (D) 39, (E) 53, and (F) 66 s after the potential was scanned to -50 mV at 2 mV s^{-1} .

Sulfur is a common impurity in Cu and, at these potentials, would be resistant to dissolution. Metallic impurities (such as a more noble metal) would also be resistant. Surface defects can affect dissolution, and a previous study has shown that screw dislocations on Au(111) were not etched when exposed to CN^- solutions.¹¹ Several authors have performed theoretical studies¹² and UHV STM studies¹³ of pinning phenomena on metal surfaces and have shown that pinning centers (caused by lattice impurities) can affect the surrounding morphology by up to several micrometers. In the case here, it is difficult to determine the exact nature of the pinning agent, but sulfur is a reasonable possibility.

If the potential of the substrate is increased from that used in Figure 1, the etching rate increases (Figure 4). The image in Figure 4A was taken at -77 mV, and the images in Figure 4B–F were obtained after sweeping the potential from -77 mV (see Figure 2) to -51 mV at 2 mV s^{-1} . Note that the etching rate increased in comparison to the rate in Figure 2. Several terraces in this series of images are of interest. T1, for example, splits into two areas after a thin slot etches into the center of the terrace. Only a small portion of T1 remains in Figure 4D. T3 undergoes a similar fate (Figure 4B); note that the T3 slot orientation is 90° from the one observed on T1. The mechanism of slot formation may involve a local defect structure that increases the rate of dissolution. We observed similar behavior for Cu(111) in 10 mM HCl .⁶ Here, an unknown surface impurity appeared to catalyze dissolution of new deeper edges which continued to etch for several minutes. As the potential increased from 0 to 30 mV, the surface became heavily etched, although the etching still occurred at $\{100\}$ edges. Pinning of step edges was frequently observed; this caused indentations to form on the steps, and as new edges were uncovered, they began to etch and become deeper and wider.

Imaging at a very high current density was possible. At 200 mV the substrate current was about $80 \mu\text{A cm}^{-2}$, and the etching rate was quite fast. This is illustrated in Figure 5, where consecutive images obtained in the constant height mode were taken at 3 s intervals. A clear atomically resolved image of the Cl adlattice is apparent, and Figure 5A shows a dissolving step edge with the individual atoms visible along the step. The mechanism was the same as that observed at lower potentials. When the crystal was visually examined under magnification after this treatment, the surface was heavily pitted and rough. However, a bright spot about 0.3 mm in diameter was observed on the surface where the tip was located. This section of the surface was pitted but not to the extent of the rest of the surface. Approximately square etch pits were observed on the bright area, and their edges were in approximately the $\{100\}$ direction as observed microscopically. Similar morphologies have been observed by scanning electron microscopy after etching a Cu(100) surface in a $4 \text{ M H}_2\text{SO}_4$, 2 M HNO_3 , and 10 mM HCl solution.¹⁵ Auger and LEED analysis of the etched surface showed an ordered $(\sqrt{2} \times \sqrt{2})R45^\circ$ Cl structure. This is consistent with the results shown here where loss of Cl was not observed at higher dissolution potentials. The presence of the spot was probably due to blocking of the surface by the bulk of the tip, resulting in a less positive potential at this location.

Cu Deposition after Dissolution and Cu(100) Reordering.

The dissolution process can be reversed by sweeping the potential in a negative direction after a dissolution experiment. Upon reversal of the potential, the $\{100\}$ edges begin to grow and re-form the terraces just etched, as illustrated in Figure 6. This surface had been subjected to a series of dissolution experiments with the last treatment at -100 mV for 4 min (following a previous one at 0 mV). The potential was then

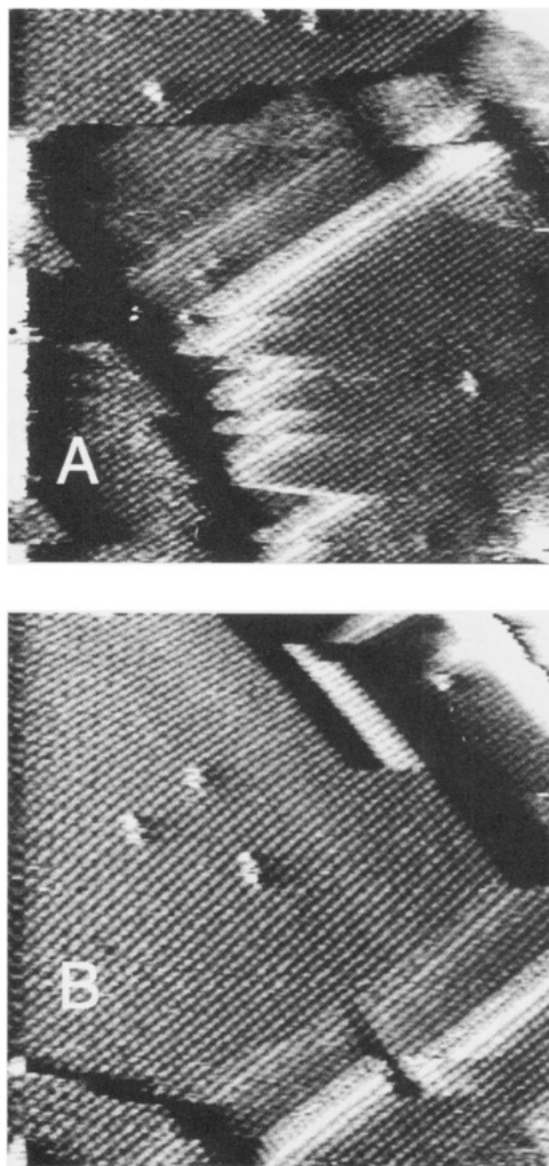


Figure 5. $20 \text{ nm} \times 20 \text{ nm}$ STM micrographs taken at 200 mV with $V_{\text{tip}} = 216 \text{ mV}$ and $i_{\text{T}} = 4.0 \text{ nA}$. The images were taken consecutively with each image taking 3 s to acquire. Note the well-defined atomic structure of the dissolving terrace in the upper portion of A.

scanned back to -300 mV at 2 mV s^{-1} . These images were captured about 20 min after this scan. Note the growth of terrace T2 (Figure 6A and B) from the outer edge of T1 and inward and toward the upper right-hand portion of the image. T1 did not advance downward until it had completely grown along T2. T1 finally caught up with T2 (Figure 6E), creating a double step. Although one would expect more three-dimensional nucleation,¹⁴ growth along a terrace appears to be faster than that at a steep, multistep edge. However, invariably, after long periods of time, the surface returned to one that was smooth. The dissolution process could then be repeated again with the $\{100\}$ edges dissolving. Step edges are known to act as nucleation sites, e.g., as seen with bulk Cu deposition on Au(111).¹⁶ The smoothing process (at long times) probably involves the diffusion of Cu atoms on the surface. This type of diffusion was previously observed for Cu(111) electrodes in 10 mM HCl ⁵ and also resulted in smoothing of the surface. This smoothing process probably is enhanced by the high mobility imparted to the copper by the adsorbed Cl^- . The Cl^- weakens the Cu–Cu interactions¹⁰ which lowers the energetic barrier for diffusion. Similar smoothing of Cu(100) surfaces was observed

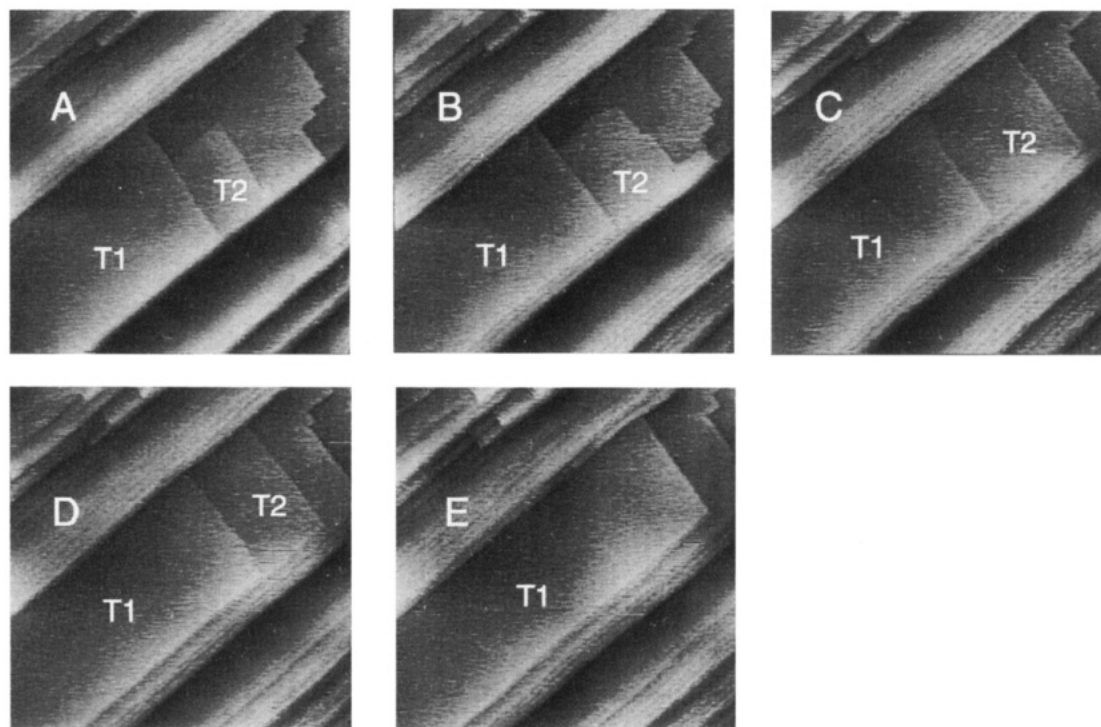


Figure 6. 80 nm \times 80 nm STM micrographs over a period of time showing the deposition of Cu at {100} step edges on Cu(100). The Cu(100) surface had been subjected to dissolution twice before these images were taken (see text). The images have been contrast-enhanced to show the step edges more clearly. The time between each image was 13 s with $V_{\text{tip}} = 0$ mV and $i_T = 9.8$ nA.

by LEED after an ion-bombarded surface was exposed to 1 mM HCl. Au(111) also smoothes out after exposure to Cl^- in 0.1 M HClO_4 with 0.1 mM HCl.¹⁷ These factors provide an explanation about why potential cycling of a Cu electrode in the dissolution/deposition region does not degrade the overall surface quality.

Cu Anodic Dissolution Mechanism in Cl^- . Previous studies of Cu in aqueous chloride at various Cl^- concentrations and pH values have shown the reaction to follow the scheme outlined below at $[\text{Cl}^-] < 1$ M.¹⁸



The initial step in the mechanism involves the adsorption of Cl^- on the surface. This is followed by another Cl^- combining with the adsorbed CuCl and diffusing into solution; the rate of diffusion of this complex away from the electrode is the rate-determining step. In the present study, the $(\sqrt{2} \times \sqrt{2})R45^\circ$ Cl adlattice is ubiquitous, even during dissolution. Figure 7 shows an atomic resolution image of a step during dissolution. We have never observed bare copper at a step edge, indicating that as soon as the CuCl complex dissolves (reaction 2), another Cl^- from solution adsorbs. Here, we further extend the concept that different sites on a surface have different reactivities.⁵

On Cu(111) the {211} edges are preferentially etched over the more stable {110} edges.⁵ This correlates well with the results presented here, since the kinked nature of the Cu(111) {211} edge is similar to that of the Cu(100) {100} direction. In fact, the Cu(100) {100} edge has a more open structure. This may account for the heavily etched surface seen at higher potentials in this study. The roughness of the etching at higher potentials may also be a function of terrace edge pinning. The pinning of step edges was also observed for Cu(111) surfaces with similar results. Overall, the Cu(100) surface is more

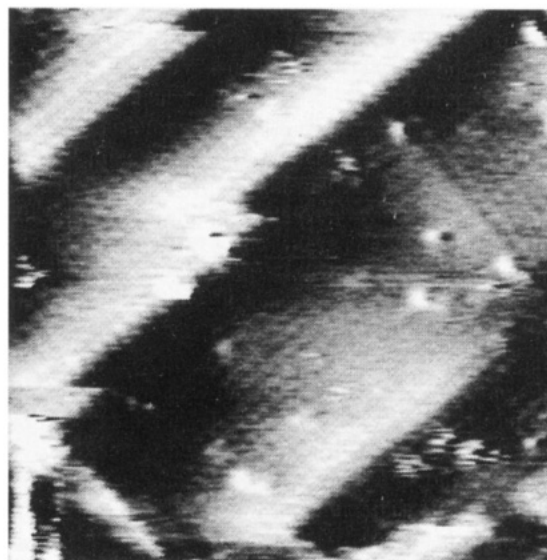


Figure 7. 17 nm \times 17 nm atomic image of a {100} step edge during dissolution at -50 mV ($V_{\text{tip}} = 0$ mV and $i_T = 5.0$ nA). These images show that the Cl is adsorbed at all points near the step edge.

reactive than the (111) surface. This can be attributed to the more open structure (lower coordination) of the surface promoting dissolution.

Conclusion

In situ STM analysis has been used to examine the anodic dissolution of Cu(111) in aqueous Cl^- solutions with atomic resolution. Cl^- adsorbs in a $(\sqrt{2} \times \sqrt{2})R45^\circ$ adlattice structure, as previously observed by LEED and in situ AFM. Cu dissolution proceeded via dissolution of step edges in 10 mM HCl. Step edges along the {100} direction were preferentially etched because of the high density of kinks and the open structure of the underlying Cu edge. Dissolution experiments

also revealed that some edges did not retreat evenly, probably because impurities (like sulfur) or lattice defects can pin edges. Dissolution at relatively high potentials caused an increase in the dissolution rate, but the step edge mechanism still prevailed. The dissolution process could be reversed, resulting in Cu deposition at the {100} edges. Smoothing of the surface occurred after longer deposition periods, probably because of the high Cu mobility imparted by the adsorption of Cl. These results support previous LEED studies that showed Cu(100) surfaces could be reordered after emersion from millimolar HCl solutions.

Acknowledgment. The support of this work by the National Science Foundation (CHE9214480) and the Robert A. Welch Foundation is gratefully acknowledged.

References and Notes

- (1) (a) *Corrosion Mechanisms*; Mansfeld, F., Ed.; Marcel Dekker: New York, 1987. (b) Sangwal, K. In *Etching of Crystals: Theory, Experiment, and Applications*; Amelinckx, S., Nihoul, J., Eds.; North-Holland: Amsterdam, 1987.
- (2) (a) Schardt, B. C.; Yau, S. L.; Rinaldi, F. *Science* **1989**, *243*, 1050. (b) Haiss, W.; Sass, J. K.; Gao, X.; Weaver, M. J. *Surf. Sci. Lett.* **1992**, *274*, L593.
- (3) *Scanning Tunneling Microscopy and Spectroscopy: Theory, Techniques, and Applications*; Bonnell, D. A., Ed.; VCH: New York, 1993; Chapter 8.

- (4) Bertocci, U.; Turner, D. R. In *Encyclopedia of Electrochemistry of the Elements*; Bard, A. J., Ed.; Marcel Dekker: New York, 1974; Vol. II, Chapter II-6.
- (5) Suggs, D. W.; Bard, A. J. *J. Am. Chem. Soc.* **1994**, *116*, 10 725.
- (6) Nagahara, L. A.; Thundat, T.; Lindsay, S. M. *Rev. Sci. Instrum.* **1989**, *60*, 3128.
- (7) Seigenthaler, H.; Juttner, K. *J. Electroanal. Chem.* **1984**, *163*, 327.
- (8) Stickney, J. L.; Ehlers, C. B.; Gregory, B. W. *Langmuir* **1988**, *4*, 1368.
- (9) Cruickshank, B. J.; Sneddon, D. D.; Gewirth, A. A. *Surf. Sci. Lett.* **1993**, *281*, L308.
- (10) Westphal, D.; Goldmann, A. *Surf. Sci.* **1983**, *131*, 113.
- (11) McCarley, R. L.; Bard, A. J. *J. Phys. Chem.* **1992**, *96*, 7410.
- (12) Chui, S. T.; Weeks, J. D. *Phys. Rev. B* **1981**, *23*, 2438.
- (13) Ozcomert, J. S.; Pai, W. W.; Bartelt, N. C.; Reult-Robey, J. E. *Surf. Sci.* **1993**, *293*, 183, and references therein.
- (14) Budevski, E. B. In *Comprehensive Treatise of Electrochemistry*; Conway, B. E., Bockris, J. O'M., Yeager, E., Khan, S. V. M., White, R. E., Eds.; Plenum: New York, 1984; Vol. 7, pp 399-450.
- (15) Villegas, I.; Ehlers, C. B.; Stickney, J. L. *J. Electrochem. Soc.* **1990**, *137*, 3143.
- (16) Batina, N.; Will, T.; Kolb, D. M. *Faraday Discuss.* **1992**, *94*, 93.
- (17) Trevor, D. J.; Chidsey, C. E. D. *J. Vac. Sci. Technol. B* **1991**, *9*, 964.
- (18) (a) Barcia, O.; Mattos, O.; Pebere, N.; Tribollet, B. *J. Electrochem. Soc.* **1993**, *140*, 2825. (b) Cooper, R. S.; Bartlett, J. H. *J. Electrochem. Soc.* **1958**, *105*, 109. (c) Lee, H. P.; Nobe, K. *J. Electrochem. Soc.* **1986**, *130*, 403. (d) Braun, M.; Nobe, K. *J. Electrochem. Soc.* **1986**, *126*, 1666.

JP943360F